

# THE BOUND MASS OF SUBSTRUCTURES IN DARK MATTER HALOS

Laurie D. Shaw<sup>1,4</sup>

Department of Physics, McGill University, Montreal QC H3A 2T8

Jochen Weller<sup>2</sup>

Department of Physics and Astronomy, University College London, Gower Street, London WC1E 6BT, UK.

Jeremiah P Ostriker<sup>1,3</sup> AND Paul Bode<sup>3</sup>

Princeton University Observatory, Princeton NJ 08544-1001

*Draft version May 6, 2019*

## ABSTRACT

We present a new definition of subhalos in dissipationless dark matter N-body simulations, based on the coherent identification of their dynamically bound constituents. Whereas previous methods of determining the energetically bound components of a subhalo ignored the contribution of all the remaining particles in the halo (those not geometrically or dynamically associated with the subhalo), our method allows for all the forces, both internal and external, exerted on the subhalo. We demonstrate, using the output of a simulation at different timesteps, that our new method is more accurate at identifying the bound mass of a subhalo. We then compare our new method to previously adopted means of identifying subhalos by applying each to a sample of 1838 virialized halos extracted from a high resolution cosmological simulation. We find that the subhalo distributions are similar in each case, and that the increase in the binding energy of a subhalo from including all the particles located within it is almost entirely balanced by the losses due to the external forces; the net increase in the mass fraction of subhalos is roughly 10%, and the extra substructures tending to reside in the inner parts of the system. Finally, we compare the subhalo populations of halos to the sub-subhalo populations of subhalos, finding the two distributions to be similar. This is a new and interesting result, suggesting a self-similarity in the hierarchy substructures within cluster mass halos.

*Subject headings:* cosmology: dark matter— galaxies: clusters: general— methods: N-body simulations

## 1. INTRODUCTION

In the current paradigm of hierarchical structure formation, satellite galaxies in clusters are associated with the remnants of dark matter halos – known as subhalos – that have, at some point in their history, been accreted and absorbed by a more massive halo. Once captured by their host (or mother) halo, subhalos are continuously eroded by the combined effects of dynamical friction and tidal stripping by the host halo core. Often a subhalo will lose a large fraction of its mass at the time of accretion, with only the dense core surviving until the present day. In studies of structure formation, it is these self-bound remnants of the original subhalo which we associate with satellite galaxies.

With the advent of high resolution cosmological simulations, we have been able to test models of hierarchical structure formation in a  $\Lambda$ CDM universe. Until the end of the last decade, it was not possible to reach the required mass resolution to enable the identification of galaxy mass halos as substructures in

clusters (White 1976; van Kampen 1995; Summers et al. 1995; Moore et al. 1996). Commonly known as the *overmerging* problem, this was mainly due to the limited mass and force resolution of the simulations used. The major causes of this problem were premature tidal disruption due to inadequate force resolution and two-particle evaporation for halos with a small number of particles (Klypin et al. 1999). Over the last 7 years, rapid advances in parallel computing, through both the improvement of hardware and the development of fast and efficient parallel algorithms, has enabled us to achieve the numerical resolution required to overcome these numerical problems and probe the subhalo populations of  $\Lambda$ CDM halos (Ghigna et al. 1998; Klypin et al. 1999; Moore et al. 1999; Okamoto & Habe 1999; Ghigna et al. 2000; Bode et al. 2001; Springel et al. 2001; Kravtsov et al. 2004b; De Lucia et al. 2004; Gao et al. 2004; Reed et al. 2005).

However, the exact definition of a ‘subhalo’ is somewhat ambiguous, and it tends to be intrinsically linked to the algorithm adopted to identify the groups of particles belonging to each subhalo in a numerical simulation. Therefore, what constitutes a substructure is often dependent on the process or quantity being investigated. For example, if one is interested in using numerical simulations to investigate the impact of substructures within gravitational lenses, and therefore sampling the projected potential field within objects, then

Electronic address: lds@ast.cam.ac.uk

<sup>1</sup> Institute of Astronomy, University of Cambridge, Madingley Road, Cambridge CB30HA

<sup>2</sup> Department of Physics and Astronomy, University College London, Gower Street, London WC1E 6BT, UK.

<sup>3</sup> Princeton University Observatory, Princeton NJ 08544-1001

<sup>4</sup> Department of Physics, McGill University, Montreal QC H3A 2T8

a geometrical definition of a subhalo is sufficient (see, for example, Hennawi et al. (2005); Hagan et al. (2005); Mao et al. (2004); Amara et al. (2006)). However, if one instead wants to study the formation and evolution of subhalos as they initially grow through accretion, are captured by larger structures, and are subsequently depleted through dynamical friction and tidal ablation, one must then search for structures in 6 dimensional phase space in order to identify statistically significant groups of particles (Taffoni et al. 2003; Hayashi et al. 2003; Kazantzidis et al. 2004; Kravtsov et al. 2004b; Gill et al. 2004b).

However, there is an additional and often dominant goal in defining ‘substructure’. In most assemblages that we call ‘galaxies’, the lifetimes of the stars that we observe (especially in the K-band) are quite long compared to their dynamical (or orbital) times in the systems in which they are found. Hence, if the purpose is to identify objects that correspond to the galaxies that we observe, then we must identify those subhalo particles that will remain together over many dynamical timescales. In this case, all the forces on a subhalo, internal and external, must be accounted for in order to identify such objects. Requiring that all particles be energetically bound, as is adopted by many authors (e.g. Ghigna et al. (2000); Springel et al. (2001); Kravtsov et al. (2004b); De Lucia et al. (2004); Gao et al. (2004); Reed et al. (2005)), can be a necessary, but is not a sufficient, condition for coherence. We will later spell out what we believe to be a more appropriate algorithm.

There are many existing algorithms for defining and identifying halos and subhalos in dissipationless N-body simulations. As noted above, some methods are essentially geometrical, others aim at finding dynamically coherent structures; all contain both dimensionless and dimensional parameters. In general, there are three levels of refinement that one can adopt. The most basic is to use a geometrical routine, such as the Friends-Of-Friends (Huchra & Geller 1982; Davis et al. 1985; Lacey & Cole 1994) or Denmax (Bertschinger & Gelb 1991; Gelb & Bertschinger 1994; Eisenstein & Hut 1998) algorithms. These use only instantaneous particle positions to group together nearby particles (defined by the FOF ‘linking length’ or the Denmax ‘smoothing length’) into localized structures. Neither method performs any type of dynamical analysis to check whether these structures are bound.

The next level of refinement is to follow a geometrical identification of halos with a procedure for determining those particles that are dynamically associated with the substructure. Essentially, we wish to separate particles belonging to substructure from the local underlying background matter belonging solely to the cluster. This we do in two stages, first removing the velocity outliers from the subhalo, and then refining the process by iteratively removing the unbound particles with the greatest total energy until only bound particles remain. This must be done iteratively to ensure that changes in the subhalo center of mass and velocity are accounted for as particles are removed. Examples of publicly available routines that use this approach include SKID (Stadel et al. 1997; Stadel 2001), BDM (Klypin et al. 1999), SUBFIND (Springel et al. 2001), VOBOZ (Neyrinck et al.

2005) and MHF (Gill et al. 2004a). In each of these, the unbinding is performed assuming the subhalo is completely isolated, i.e. only the bound particles in the subhalo at each iteration are taken into consideration when calculating the potential energy. Not taken into account in this energy calculation are the (previously identified) unbound particles located spatially within the subhalo, nor the disruptive effect of the tidal forces from the particles surrounding it. Therefore, in order to correctly identify halos and subhalos that are not only instantaneously bound, but will also remain so in the near future (i.e. within the local dynamical timescale), one should account for all of the forces that may influence the dynamical state of a subhalo.

An instructive analogy is provided by the stars within the Milky Way. There are a significant number of stars that, by chance, have an extremely low velocity relative to that of the Sun. Consider one such star and the Sun as a single and isolated system, ignoring the effect of all the other matter in the Milky Way: by calculating the total energy of each star, it would appear that they are gravitationally bound and therefore make up a binary pair. It is only once we also take into account all the other stars in the Milky Way that we realize that the gravitational force between the star in question and the Sun is dwarfed by the tidal forces due to all the other stars in the galaxy. It then becomes clear that the two stars do not constitute a stable and bound system. The same argument may be applied to dark matter substructures in a cluster – we must take into account all the forces on a subhalo, including the tidal force from nearby subhalos and the host halo core, in order to determine whether or not it truly is a bound system. Hence, previous algorithms, which do not do this, do not provide a complete picture.

The final refinement to be made, therefore, is to account for all the remaining forces on each particle in the subhalo. In order to do this we must now include the effect of the unbound particles on the potential energy of each subhalo during each iteration of the unbinding, and then calculate the tidal force on each particle in the subhalo due to the rest of the particles in the halo. The former is a simple change to the unbinding algorithm. Computing the tidal force on each subhalo particle, however, is a more complex and costly procedure, especially in higher resolution halos. Since gravitational forces are linear, we can determine the total force on a particle as the sum of three terms:

1. forces due to the particles in the unit considered,
2. forces due to particles within the unit considered, but not bound to that unit,
3. forces due to particles outside of the unit considered.

In this paper we describe a fast algorithm we have developed in order to approximate the external tidal forces on a substructure. For the first time, we present a ‘coherent’ definition of a subhalo that accounts for all the forces it is subjected to, both internal and external, and thus identify all particles that are not just instantaneously bound to the substructure, but will remain so within the local dynamical timescale. We henceforth refer to

the method of identifying substructures used in previous studies as the *standard* subhalo definition. Essentially, these use the forces included in the first term above. We refer to the new approach outlined in this study as the *coherent* subhalo definition, allowing for the forces due to all three terms above. This is for the purpose of identifying the groups of particles that remain together over many dynamical timescales, and thus correspond to the luminous galaxies they host.

In Section 2, we summarize the main steps of the algorithm common to both procedures (see Weller et al. (2005) for a complete description), and describe in detail the routine we have developed to calculate the tidal forces on each particle in a subhalo. We then demonstrate the impact of each stage of the *standard* and *coherent* subhalo definitions on the substructure populations for a single test halo. In the last part of this section, we assess the accuracy of each method by tracking a small sample of subhalos over several timesteps, checking whether the particles identified as bound by each definition actually do stay with the subhalo over time. In Sec. 3, we then compare the mass and radial distributions of substructures for a large sample of halos analyzed using both definitions. We also look at the mass contained within subhalos of subhalos – or sub-substructures – in each sample to compare the subhalo populations of successive generations of subhalos in cluster-mass halos.

## 2. DEFINITION OF SAMPLE

### 2.1. The Identification of Halos and Subhalos

In our preceding study (Shaw et al. 2006), we presented a comprehensive analysis of the physical characteristics of a large sample of cluster mass halos. In order to compare our results with previous work, we adopted the *standard* subhalo definition, as outlined in Weller et al. (2005). This algorithm was applied to a  $\Lambda$ CDM N-body simulation of  $1024^3$  particles with box size  $320h^{-1}$  Mpc, particle mass ( $m_p$ ) of  $2.54 \times 10^9 h^{-1} M_\odot$  and a spline kernel force softening length of  $\epsilon = 3.2h^{-1}$  kpc. The simulation was evolved to  $z=0.05$  using the Tree-Particle-Mesh (TPM) algorithm (Bode & Ostriker 2003). The cosmological parameters used include  $\Omega_m = 0.3$ ,  $\Lambda = 0.7$ , and  $\sigma_8=0.95$ ; outputs from this run have previously been used to make predictions concerning strong lensing (Wambsganss et al. 2004; Hennawi et al. 2005; Das & Ostriker 2006). We wish to ensure that all the halos are well resolved and that the overmerging problem is not in evidence. Thus we discard all halos with a virial mass less than 10,000 particles ( $\approx 3 \times 10^{13} h^{-1} M_\odot$ ).

The method described in Weller et al. (2005) starts with the hierarchical identification of structures. First, cluster mass halos are identified in the simulation box using a Friends-of-Friends routine with a linking length of  $b = 0.2\bar{n}^{-1/3}$ , where  $\bar{n}^{-1/3}$  is the mean inter-particle separation. The Denmax routine of Bertschinger & Gelb (1991) is then run once on each FOF halo, using a high resolution smoothing length of  $5\epsilon$  in order to identify the substructures. A family tree is then constructed by hierarchically associating the smallest mass subhalos with their lowest mass ‘ancestor’, so that each subhalo has only a single immediate parent. Those that consist of less than 30 particles are dissolved into their immediate

parent.

Up until this point the analysis is purely geometrical. Next, we must refine our identification of subhalos by determining their dynamically bound constituents. This is achieved in two stages: as a first approximation we calculate the center of mass velocity of each subhalo and remove those particles that are statistical outliers (see Section 2.2.1 in Weller et al. 2005). This step efficiently removes the most unbound particles in each subhalo, thus allowing a more accurate determination of the subhalo center of mass velocity. We then complete the calculation exactly by iteratively identifying those particles with a total energy greater than zero (in the center of mass frame of the subhalo) and removing the most energetic. At this point the *standard* and *coherent* subhalo definitions diverge. In the former, once a particle is identified as ‘unbound’ ( $E_{bind} > 0$ ), it is removed entirely from future iterations of the calculation, and therefore its contribution to the gravitational potential energy of the substructure is neglected. This is the procedure that is adopted in the unbinding step by many publicly available codes. However, in the *coherent* halo definition, we include the contribution of the unbound particles within the subhalo. This has the effect of increasing the overall binding energy of a subhalo, reducing the number of unbound particles that are identified. In either approach we dissolve a subhalo into its immediate parent if at any stage its mass drops below 30 particles.

In both procedures, we next check to see if pairs of the immediate daughters of a parent cluster halo are bound. If this is the case, they form a *hyperstructure*; the less massive of the two becomes a daughter of the more massive structure. If a hyperstructure is found, we then check to see whether nearby particles previously not associated with either of the subhalos are bound to it. For the standard method of analyzing halos, we finally remove all subhalos and any particles that are not bound to the entire structure and the procedure is complete. However, in our coherent subhalo definition, we now allow for the tidal forces on the subhalo due to the external mass in the cluster; a full description of how this is implemented is presented in the following section. Once this is done, we finally remove unbound particles and subhalos from the cluster, as in the standard analysis.

As described in Weller et al. (2005), both procedures are both stable and largely independent of arbitrary parameter choices. Henceforth, we refer to the most massive structure in each cluster as the ‘mother’ or ‘host’ halo. We will quote the mass of the entire cluster in terms of its virial mass,  $M_{vir}$ . For a  $\Lambda$ CDM cosmology, it is conventional to define the virial mass  $M_{vir}$  and radius  $R_{vir}$  as  $M_{vir} = \frac{4}{3}\pi R_{vir}^3 \Delta_c(z) \rho_c(z)$ , where  $\rho_c$  is the critical density of the universe, and the mean over-density  $\Delta_c = 178\Omega_m(z)^{0.45}$  (Lahav et al. 1991). In order to calculate the virial mass of each mother halo, we start at its density maximum and proceed outward until we reach the virial radius, within which the mean over-density is  $\Delta_c$ ; we include all substructures with centers of mass within the virial radius. Hence we define a particle as being part of the halo if it either belongs solely to the mother halo or is part of a bound subhalo that has its center of mass within the virial radius of the mother. A flowchart of all the main steps in the coherent subhalo definition can be viewed in Fig. 1.

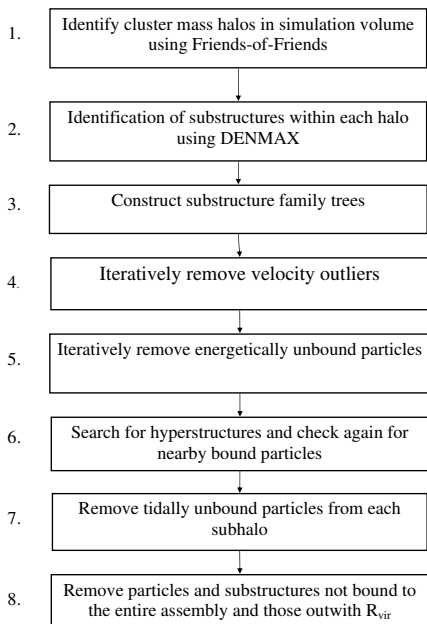


FIG. 1.— Flowchart summarizing the main steps in the identification of subhalos – according to our new *coherent* subhalo definition – in cluster mass halos extracted from dissipationless cosmological N-body simulations.

## 2.2. Calculation of external forces: the tidal approximation

For a subhalo well separated from its mother halo, the tidal radius  $R_t$  is given by (Binney & Tremaine 1987)

$$R_t = r_d \left( \frac{M(R_t)}{3M(r_d)} \right)^{1/3}, \quad (1)$$

where  $r_d$  is the distance between the density peak of the mother structure and the density peak of the substructure,  $M(r_d)$  is the mass of all the particles within this radius and  $M(R_t)$  is the mass of all the particles within the tidal radius (measured from the center of the subhalo). This formula simply asks if a particle feels a tidal force pulling it away from the substructure larger than the force pulling it to the center of the substructure. However, this equation does not apply for most halos under consideration here, since they are well *within* the mother halo. We note that Kim & Park (2006) have recently developed a routine that uses the tidal radius to demarcate subhalo regions.

Thus, in order to decide if a particle in a daughter halo will be tidally removed, we must first calculate the tidal force as the difference between the force on the particle and the force on the density peak of the daughter:

$$\mathbf{F}_{\text{tid}} = \mathbf{F}_p - \mathbf{F}_d, \quad (2)$$

where for  $\mathbf{F}_p$  and  $\mathbf{F}_d$  we sum up the force of all particles from the mother structure, including all other daughters, outside a radius  $R_t$ . Particles within the tidal radius are not contributing to the tidal (i.e. external) force. In order to decide if a particle is tidally bound we calculate the

energy

$$E_{\text{tid}} = \int_t^{t+\tau} \mathbf{F}_{\text{tid}}(t') \cdot \mathbf{v}_{\text{rel}}(t') dt' \approx \mathbf{F}_{\text{tid}}(t) \cdot \mathbf{v}_{\text{rel}}(t) \tau, \quad (3)$$

where  $\mathbf{v}_{\text{rel}}$  is the velocity of the particle relative to the center of mass of the daughter, and  $\tau$  is a characteristic time. As the characteristic time, we use one fifth of the smaller period of either the particle’s orbit around the center of the daughter halo or the daughter halo’s orbit around the center of the mother; this is the interval over which the tidal force would be approximately constant. This requirement ensures that there is little scope for varying  $\tau$  as a free parameter. Eqn. 3 thus gives an approximation for the energy gain of a particle due to the tidal force in the interval before this force changes substantially. If a particle has

$$E_{\text{tid}} + E_{\text{tot}} > 0, \quad (4)$$

we declare the particle tidally unbound and move it to the associated mother. However with this criterion a small number of particles far from the substructure might be considered bound even when the tidal force is large, should its velocity by chance be perpendicular to the tidal force, leading Eqn. 3 to give a zero tidal energy. We avoid this problem if we include an additional criterion:

$$\mathbf{F}_{\text{tid}} \cdot \left( \frac{\delta \mathbf{r}}{|\delta \mathbf{r}|} \right) > \frac{8}{3} \frac{GM(|\delta \mathbf{r}|) m_p}{|\delta \mathbf{r}|^2}, \quad (5)$$

where  $\delta \mathbf{r}$  is the position of the particle relative to the central density peak of the daughter, and  $M(|\delta \mathbf{r}|)$  is the mass within the daughter up to this radius. This is a relaxed version of the tidal radius criterion in Eqn. 1, and corresponds to the particle being at twice the tidal radius if the two halos are spatially separated. We declare particles to be tidally unbound if they fulfil either Eqn. 4 or Eqn. 5.

A problem with the prescribed scheme above is that in order to calculate the tidal force for each particle we need to perform a costly  $N^2$  operation. However, since an approximate correction for the tidal force will suffice, we calculate  $\mathbf{F}_{\text{tid}}$  with a linear approximation in the following way. We consider a cube with its center at the density peak of the daughter and a side length of  $2R_t$  as in Fig. 2. We calculate the tidal force exactly at the center of each of the six faces of the cube. We then perform a linear fit to calculate the tidal force at the center of the each of the faces with

$$\mathbf{F}_{\text{tid}} = \mathbf{A}(\mathbf{r}_p - \mathbf{r}_d), \quad (6)$$

where  $\mathbf{r}_d$  is the peak density position of the daughter (relative to the peak density position of the mother halo), and the entries of the  $3 \times 3$  matrix  $\mathbf{A}$  are obtained by a least squares fit of the exact tidal force at the center of the 6 faces. This approximation corresponds to a divergence free field and hence to a quadrupole approximation, and works well when the tidal radius of the daughter is sufficiently small compared to the distance between the density peak of the daughter and the mother. We use the approximation if  $R_t/|\mathbf{r}_d| < 0.5$ ; otherwise we switch to an exact  $N^2$  calculation. We found that the median error due to the linear tidal force approximation was about 20%.

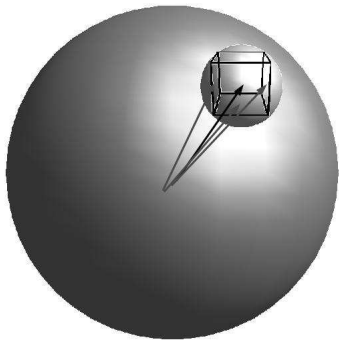


FIG. 2.— Schematic description of the quantities for the calculation of the tidal radius. The big sphere represents the mother halo, and the small the daughter. The dark arrow in the middle is the vector to the density peak of the daughter. The box represents the face of the cube of length  $2R_t$  which we use to calculate the approximate tidal forces. The light arrows illustrate three of the positions used to calculate the forces at the faces of the cube.

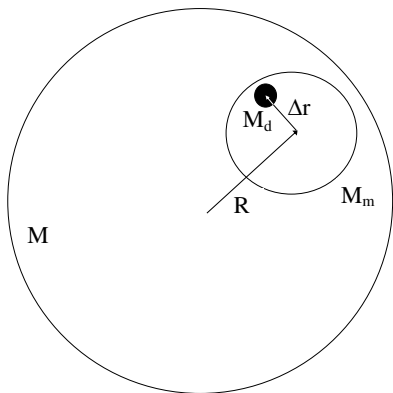


FIG. 3.— Schematic representation of the quantities required to establish if a daughter is tidally bound.

The next step is to remove tidally unbound daughters from structures. From the point of view taken here, none of the daughters can be tidally removed from the entire cluster, because we are unable to calculate the tidal forces from the mass distribution surrounding it. So this step will not change the total amount of substructure in the halo, but it might reduce the size of hyperstructures. The criterion to determine if a daughter is tidally bound to another substructure is

$$\Delta r \leq R \left( \frac{m_d + m_M}{3M} \right)^{1/3}, \quad (7)$$

with  $M$  the mass of the mother of the substructure,  $m_M$  the mass of the substructure,  $m_d$  the mass of the daughter of the substructure,  $R$  the distance from the mother to the density peak of the substructure, and  $\Delta r$  the distance between the substructure and the density peak of the daughter. These quantities are schematically represented in Figure 3.

### 2.3. Application to a Single Halo

In order to compare the standard and coherent halo definitions, in Table 1 we give for each step the number of particles ( $N_p$ ), the number of subhalos and the fraction of mass contained in substructure ( $f_s$ ) for one of the most massive halos in our sample, analyzed using both methods. The first line in the table gives the properties of the halo at the point just prior to where the two methods diverge – after the initial geometrical identification of subhalos using DENMAX and having removed the velocity outliers from each subhalo (see Weller et al. 2005). During the following two stages – the unbinding and identification of hyperstructures – over half the substructure is removed in both methods. However, at this point there is nearly 77% more substructure in the halo with the coherent analysis relative to the standard. This is because in the coherent analysis the unbound particles are retained in the potential calculation (but ignored in the standard analysis). Therefore, the gravitational potential experienced by each particle is greater, thus decreasing the number of particles identified as being ‘unbound’. However, once the tidally unbound particles have been removed, the fraction of mass contained in substructure is only slightly greater for the coherent analysis.  $N_p$ ,  $f_s$  and the number of subhalos all decrease further in the final stage as particles and subhalos not bound to the entire cluster, or those that are outwith the virial radius, are removed (see the last line of Table 1).

Fig. 4 displays projections of the density of substructure particles in the halo after each step in Table 1. The greater mass of subhalos after the unbinding step in the coherent analysis relative to the standard analysis is evident, as is the impact of the tidal step.

### 2.4. Tracking Subhalo Mass

We have described a new method for defining and measuring the bound mass of substructures in N-body simulations. However, in order to demonstrate decisively that our ‘coherent’ scheme is an improvement on the standard procedure, we must show that the particles it identifies as ‘bound’ are still associated with the subhalo at a later time, and that it is more accurate in doing so. Likewise, we must demonstrate that the particles identified as ‘unbound’ are not associated with the subhalo at future timesteps.

To perform this test, we use the output of a  $256^3$  particle simulation (with particle mass  $m_p = 3.15 \times 10^7 h^{-1} M_\odot$ ) in a box of side-length  $19.25 h^{-1} Mpc$  and a (spline) softening length of  $2.5 h^{-1} kpc$ . We adopt a  $\Lambda$ CDM cosmology, with  $\Omega_\Lambda = 0.733$ ,  $H_0 = 71 km s^{-1} Mpc^{-1}$  and  $\sigma_8 = 0.84$ . The output of this simulation was saved after every 10 particle-mesh timesteps

|                                       | Coherent Analysis |       |       | Standard Analysis |       |       |
|---------------------------------------|-------------------|-------|-------|-------------------|-------|-------|
| Step                                  | $N_p$             | $f_s$ | Nsubs | $N_p$             | $f_s$ | Nsubs |
| Denmax                                | 472659            | 34.8% | 2185  | 472659            | 34.8% | 2185  |
| Subhalo unbinding and Hyperstructures | 472659            | 8.4%  | 61    | 472659            | 4.75% | 56    |
| Tidal Step                            | 472659            | 5.2%  | 58    | n/a               |       |       |
| Cluster unbinding and virial cut      | 402411            | 4.5%  | 43    | 402534            | 4.0 % | 41    |

TABLE 1

COMPARISON BETWEEN SUBHALO DEFINITIONS OF THE SUBSTRUCTURE CONTENT OF HALO 1 AFTER THE COMPLETION OF EACH STEP IN THE RESPECTIVE PROCEDURES.

(see Table 2); henceforth, we refer to the time elapsed between each saved output as being one ‘timestep’. Each particle was allocated a unique identifier number at the beginning of the simulation, to enable us to track individual particles over time. Although this simulation contained fewer particles than our main  $1024^3$  simulation, the smaller box size ensured that we could easily locate and follow a small number of well resolved cluster-mass halos.

In each of the final six outputs of the simulation (from  $z = 0.13$  to 0, or a time period of 1.17 Gyrs) we identified all structures of mass greater than  $10^{13}M_\odot$  using the procedure outlined in Sec. 2.1. From this sample we selected the most massive halo possessing a stable mass – one in which the mass fluctuates by less than 5% – over the time-period considered. The main physical properties of this halo can be viewed in Table 2. We also checked to make sure that the halo did not undergo any major mergers during this period.

At each timestep, we applied both the standard and coherent subhalo definitions to identify the substructure populations of the halo. For each subhalo we identify five sets of particles. The set  $D_i$  contains all the particles geometrically associated with a subhalo, as identified by the DENMAX step (step 2 in Figure 1), at time  $t_i$  (where the index  $i$  indicates the timestep). The subset  $U_i$  contains all the particles that were associated with a subhalo by the DENMAX routine (i.e. that are in  $D_i$ ) but were then removed during the unbinding stages. The subset  $B_i$  contains all particles that remained in the subhalo at the end of our entire routine – these are the ‘bound’ particles. Hence, for each subhalo we have five sets at each timestep;  $D_i$ , which is of course defined before the binding criteria are applied and so is the same for both the standard and coherent definitions,  $U_i$  and  $B_i$  as determined by the standard definition and  $U_i$  and  $B_i$  as determined by the coherent. The number of particles in any set  $S_i$  is written  $N(S_i)$ . For example, the total number of particles associated with a subhalo at a particular timestep is  $N(D_i) = N(U_i) + N(B_i)$ .

To achieve our aim of following the bound constituents of a subhalo, we must be able to identify the same subhalo at a later time. This is more complicated than simply matching up particle id tags; over the course of time,

subhalos may dissolve (by dropping below the 30 particle limit), merge, fragment, or temporarily move outwith the virial radius of the cluster or disappear into its core where DENMAX is unable to locate them. Hence, to achieve a one-to-one correspondence between subhalos at two different times requires a clear definition of how to identify its descendant. To resolve this issue we developed a simple matching algorithm that identifies the descendant of a subhalo when there might be some ambiguity. This routine operates by pairing the most massive progenitor with its most massive descendant, should there be more than one in either case.

At each timestep considered,  $t_i$ , we look for the same subhalo at the subsequent timestep  $t_{i+1}$ . We do this for both the standard and coherent methods. If no descendant at the subsequent timestep is found for a particular subhalo for either method it is removed from the sample. This ensures a consistent comparison between the two methods (i.e. the same subhalos are being compared). Normally, a subhalo will only permanently disappear if it drops below the 30 particle minimum mass and is dissolved into its immediate parent. For each subhalo, we are now able to calculate quantities such as  $N(B_i \cap B_{i+1})$ , or the total number of particles that are found to be bound to the subhalo at *both*  $t_i$  and  $t_{i+1}$ .

We now define three quantities (to be measured for each subhalo) that can be used to assess the accuracy of each criterion:

- The probability  $P_b$  that a particle in the subhalo is contained in the ‘bound’ set  $B_i$  but is *not* in the ‘bound’ set  $B_{i+1}$  at the subsequent timestep (written  $\bar{B}_{i+1}$ ):

$$P_b = \frac{N(B_i \cap (\bar{B}_{i+1}))}{N(D_i)}. \quad (8)$$

Note that  $\bar{B}_{i+1} \neq U_{i+1}$ . This is because  $U_{i+1}$  includes only those particles that are geometrically associated to a subhalo at  $t_{i+1}$ , but were removed from the subhalo during the unbinding stages.  $\bar{B}_{i+1}$  includes any particle in the entire *halo* that is not bound to the subhalo in question at  $t_{i+1}$ .

- The probability  $P_u$  that a particle in the subhalo

| step | z    | $t_{lookback}$<br>[Gyrs] | $M_{halo}$<br>[ $h^{-1}M_{sun}$ ] | $N_{sub}$ (coh) | $N_{sub}$ (std) |
|------|------|--------------------------|-----------------------------------|-----------------|-----------------|
| 35   | 0.13 | 1.17                     | $1.40 \times 10^{13}$             | 59              | 58              |
| 36   | 0.1  | 0.92                     | $1.41 \times 10^{13}$             | 56              | 56              |
| 37   | 0.07 | 0.66                     | $1.43 \times 10^{13}$             | 56              | 55              |
| 38   | 0.05 | 0.48                     | $1.44 \times 10^{13}$             | 57              | 54              |
| 39   | 0.02 | 0.19                     | $1.45 \times 10^{13}$             | 60              | 50              |
| 40   | 0    | 0.00                     | $1.46 \times 10^{13}$             | 60              | 52              |

TABLE 2

MASS AND THE NUMBER OF SUBHALOS (AS IDENTIFIED BY THE STANDARD (STD) AND COHERENT (COH) METHODS) IN A HALO FOLLOWED OVER THE FINAL 6 STEPS OF A  $256^3$  PARTICLE SIMULATION (DISCUSSED IN SECTION 2.4).

is contained in the ‘unbound’ set  $U_i$  but is found in the ‘bound’ set  $B_{i+1}$  at the subsequent timestep:

$$P_u = \frac{N(U_i \cap B_{i+1})}{N(D_i)}, \quad (9)$$

- The error on the bound mass determination for a subhalo,

$$\epsilon_m = \frac{N(B_i) - N(B_{i+1}|D_i)}{N(D_i)}, \quad (10)$$

or in words, the fraction of particles that were labelled ‘bound’ at  $t_i$ , minus the fraction of particles from the total set  $D_i$  that actually *were* bound (i.e. are also found in  $B_{i+1}$ ).

The reason why we must write  $(B_{i+1}|D_i)$  is that subhalos sometimes ‘sweep up’ particles from the mother halo between timesteps. Of course, these particles cannot be accounted for by either criteria – we therefore ignore them in this analysis.

If a criterion for identifying the bound mass component of subhalos in simulations claimed to operate perfectly, we might expect to find  $P_b = 0$  (particles that we say are bound, do actually stay bound),  $P_u = 0$  (particles that we say are unbound move away) and  $\epsilon_m = 0$  (the number of particles identified as bound at  $t_i$  is the same as the number identified as bound at  $t_{i+1}$ , ignoring particles picked up along the way). In practice, within one timestep a subhalo may undergo a close encounter with another subhalo or the host halo core and therefore lose particles due to physical processes that cannot be accounted for by applying dynamical criteria at each timestep. However, these effects will apply equally to subhalos identified by both methods, and thus will not affect our study of their relative accuracy.

In Figures 5, 6 and 7 we plot the distribution of each of these quantities for the full sample of subhalos followed over a single timestep (i.e.  $i = 35-36, 36-37$ , etc). This is equivalent to 0.23 Gyrs, or 2.88 times the average characteristic dynamical time ( $\tau$  in Section 2.2). It is clear from the distributions of  $P_b$  in Figure 5 that the coherent definition (dashed line) is less likely to mislabel as

‘bound’ a particle that does not remain with a subhalo than the standard definition (solid line). The mean value of  $P_b$  for the standard sample ( $0.089 \pm 0.006$ , where the error is the standard error in the mean) is 28% greater than that for the coherent sample ( $0.070 \pm 0.004$ ). Hence, the standard routine is less successful at removing particles that are not bound to the subhalo. However, both methods do equally well at correctly identifying the unbound particles – the mean value of both distributions in Figure 6 is  $\langle P_u \rangle = 0.007$ .

The distributions of  $\epsilon_m$  in Figure 7, which are largely greater than zero, suggest that both methods overestimate the bound mass of a subhalo. However, it is clear that the error is significantly less for the coherent definition ( $\langle \epsilon_m \rangle = 0.015 \pm 0.002$ , dashed line/arrow) than the standard subhalo sample ( $\langle \epsilon_m \rangle = 0.022 \pm 0.002$ , solid line/arrow). Again, this demonstrates that the standard routine is less accurate at identifying and removing unbound particles and thus provides a less reliable measure of subhalo mass.

We now investigate the accuracy of each method as a function of time (number of timesteps). This is achieved by also matching subhalos to their descendants between two and five timesteps later (equivalent to 0.473 – 1.17 Gyrs, or 2.88 - 14.6 characteristic dynamical times) and determining the fraction of particles in each subhalo at  $t_i$  that were correctly identified as being bound or unbound. In Figures 8 and 9 we analyse  $\epsilon_m$  and  $P_b$  as a function of the time between outputs ( $\Delta t$ ). In the upper panel of both plots, each point represents the mean values (and the standard error in the mean) of  $\epsilon_m$  and  $P_b$  respectively, for the sample of subhalos followed over 1-5 timesteps. Hence, the left-most point in the upper panel of Figure 8 represents the mean value of  $P_b$  measured over a single timestep (as marked by the arrows in Figure 5), the second point over two timesteps, and so on. As usual, the dashed line represents the results obtained for the coherent sample; the solid line those obtained for the standard sample.

As expected,  $P_b$ , the probability that a particle labelled as ‘bound’ at time  $t_i$  has left the subhalo at a later time  $t_{i+j}$  (where  $j=1-5$ ), increases as  $\Delta t$  increases

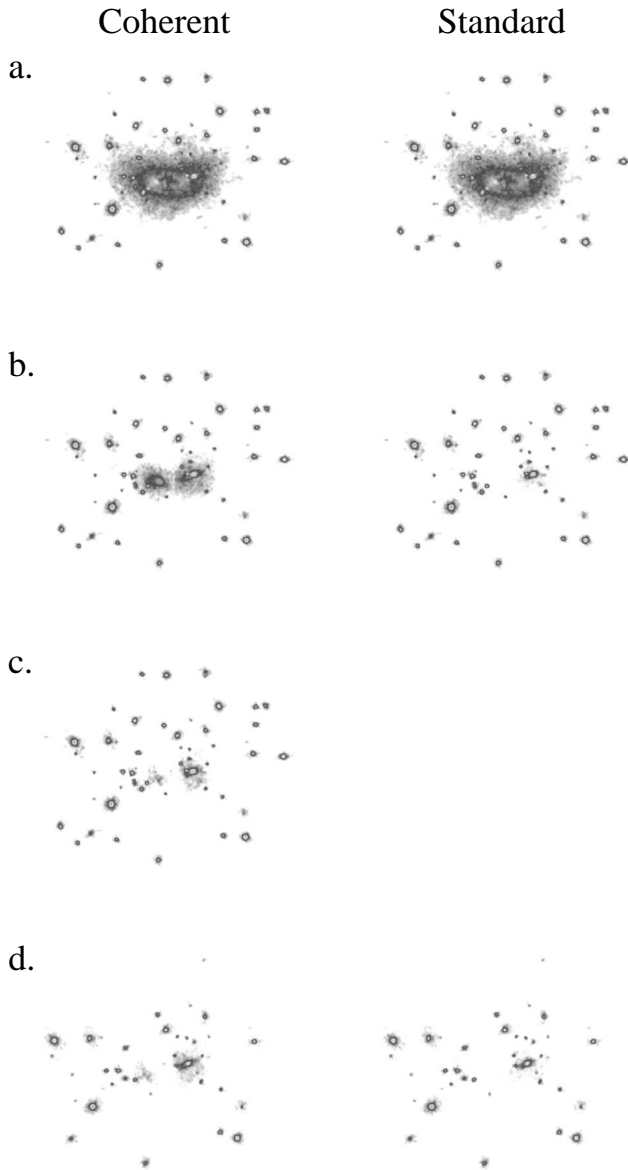


FIG. 4.— 2d projection of the substructure in one of the most massive halos in our sample after the completion of each stage of the analysis for both the *standard* and *coherent* halo definitions: after the denmax step and removal of the velocity outliers (a), the unbinding and identification of hyperstructures (b), the removal of tidally inbound particles (c) and, finally, having removed particles and subhalos unbound to the entire structure (d).

for both methods (see Figure 8). After a single timestep ( $\approx 0.23$  Gyrs),  $P_b = 0.07$  and  $0.09$  for the coherent and standard methods respectively. When measured over five timesteps (1.17 Gyrs), this increases to  $0.25$  and  $0.28$ . The lower panel, which charts the difference in the value of  $P_b$  obtained between the standard and coherent method, demonstrates that the coherent procedure becomes increasingly more accurate with respect to the standard with larger  $\Delta t$ . A similar result is demonstrated in Figure 9, where we plot  $\epsilon(\Delta t)$ . Gradually, particles identified as ‘bound’ by each method are removed from the subhalo by dynamical friction or tidal stripping, and so the error on the predicted subhalo mass at  $t_i$  grows with  $\Delta t$ . However, as discussed above, the increase in  $\epsilon$  and  $P_b$  will be partly due to interactions with other

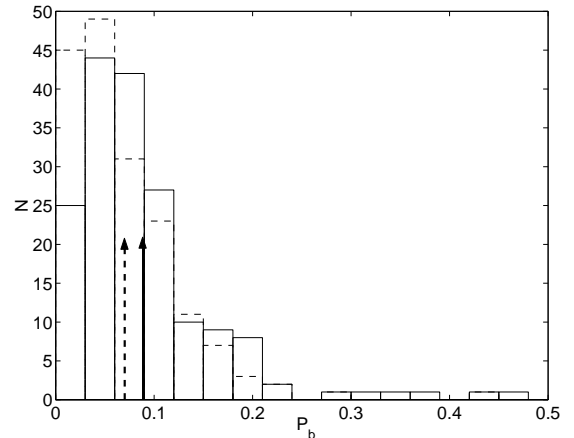


FIG. 5.— The distribution of  $P_b$  (see Section 2.4) for the coherent (dashed) and standard (solid) subhalo samples, measured over a single timestep. The arrows mark the mean values of each distribution, respectively. It is clear that the coherent method is less likely to mislabel as ‘bound’ particles that in fact leave the subhalo.

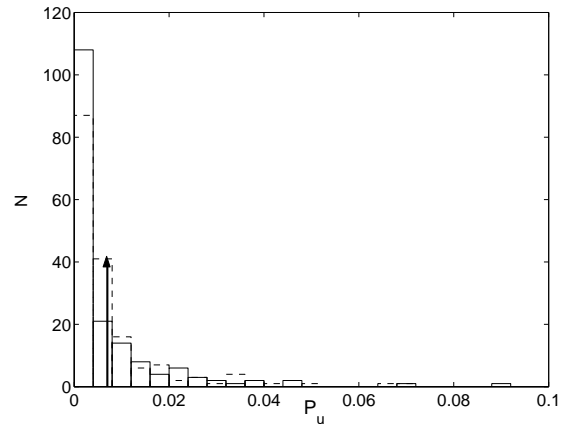


FIG. 6.— The distribution of  $P_u$  (see Section 2.4) for the coherent (dashed) and standard (solid) subhalo samples, measured over a single timestep. The arrow marks the mean values (which are the same) of both distributions. On average, the results indicate that, for both methods, less than 1% of the particles identified as ‘unbound’ are actually bound to (and thus remain with) the subhalo.

subhalos or the cluster core within the time period over which they are evaluated and therefore is not solely due to inaccuracies in either method. Nevertheless, the errors for the standard method grow slightly more rapidly than for the coherent.

Overall, although both methods do well at determining those particles that are bound to a subhalo and those that will soon move away, we have clearly demonstrated that our new coherent method provides the more precise measure of subhalo mass. Whilst both the standard and coherent definitions overestimate subhalo masses, the latter is less prone to mistakenly labelling ‘unbound’ particles as ‘bound’. It is important to note that the improvement is evident despite the 20% error in the tidal forces due to the approximate scheme that we use to evaluate them (see Section 2.2). Additionally, at any instant, we are only able to determine those particles that will be removed by tidal forces within a single characteristic dynamical timescale ( $\langle\tau\rangle \approx 0.08$  Gyrs =  $0.35$  timesteps), as described in Section 2.2. We therefore do not expect



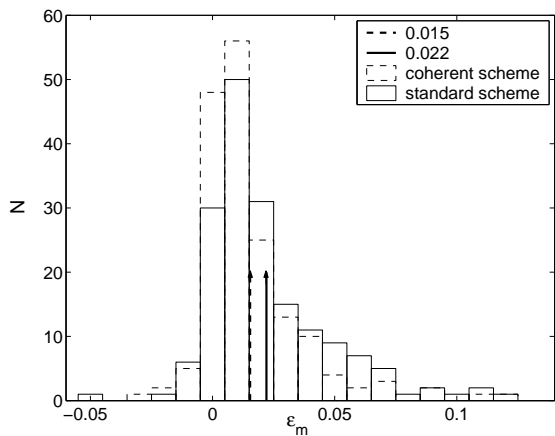


FIG. 7.— The distribution of  $\epsilon_m$  – the error on the bound mass determination for each subhalo – (see Section 2.4) for the coherent (dashed) and standard (solid) subhalo samples, measured over a single timestep. The arrows mark the mean values of each distribution, respectively. The coherent method is clearly more accurate at measuring the bound mass of a subhalo than the standard method.

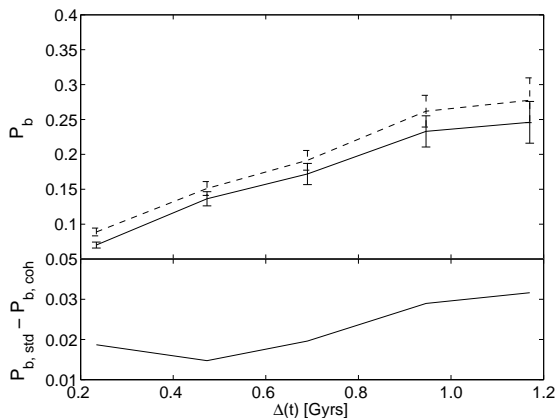


FIG. 8.— (*upper*) The mean value of  $P_b$  obtained when measured over 1-5 timesteps ( $\Delta t = 0.23 - 1.17$  Gyrs, or 2.88 - 14.6 characteristic dynamical times) for the standard (solid) and coherent (dashed) subhalo definitions. Error bars denote the standard error in the mean. (*lower*) The difference between the mean values of  $P_b$  measured for the standard (std) and coherent (coh) methods as  $\Delta t$  increases.

our coherent definition to be significantly more accurate than the standard scheme over timescales longer than a few dynamical times.

Furthermore, to perform this analysis we picked a halo that contained a typical fraction of its mass in substructure ( $\approx 7\%$ ). If we had chosen a halo that contained several large substructures (i.e. a halo undergoing a major merger) then the tidal forces exerted on each subhalo would have been more substantial, requiring a larger correction to their bound mass.

### 3. COMPARISON BETWEEN METHODS FOR A LARGE HALO SAMPLE

Both the standard and coherent subhalo definitions were applied to the 2000 most massive halos extracted from the large  $1024^3$  particle simulation described in Section 2.1. Using the procedure described in Shaw et al. (2006) we removed from each sample those halos that are not ‘virialized’, that is, have not yet reached a state of dynamical equilibrium; there then remains 1838 ha-

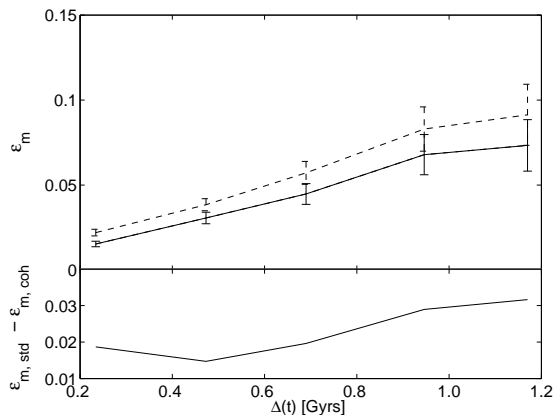


FIG. 9.— (*upper*) The mean value of  $\epsilon_m$  obtained when measured over 1-5 timesteps ( $\Delta t = 0.23 - 1.17$  Gyrs, or 2.88 - 14.6 characteristic dynamical times), for the standard (solid) and coherent (dashed) subhalo definitions. Error bars denote the standard error in the mean. (*lower*) The difference between the mean values of  $\epsilon_m$  measured for the standard (std) and coherent (coh) methods as  $\Delta t$  increases.

los in each sample. In the following Section we compare the subhalo populations and their radial distributions for each sample, and finally we investigate the subhalo populations of *subhalos*.

#### 3.1. Substructure Populations of Halos

Since the force and mass resolution of N-body simulations has reached a high enough level to enable the identification of subhalos within larger structures, several previous studies have attempted to measure the slope of the subhalo mass function (SMF). This is especially important if one wishes to quantify the relationship between the properties of dark matter subhalos identified in simulations and observed properties of galaxies (see for example Kravtsov et al. 2004a; Tasitsiomi et al. 2004; Vale & Ostriker 2006). Studies of small numbers of halos selected from low resolution simulations and resimulated at higher resolutions have suggested that dark matter halos are self-similar in terms of their subhalo populations: low mass halos appear like ‘rescaled versions’ of higher mass halos (Moore et al. 1999; Ghigna et al. 2000; De Lucia et al. 2004; Reed et al. 2005). However, recent studies of much larger samples have found evidence that this is not the case – higher mass halos contain more substructure, as they have formed more recently and have therefore had less time in which to disrupt their hosted subhalos (Gao et al. 2004; Kang et al. 2005; Shaw et al. 2006).

In Fig. 10 we compare the differential subhalo mass functions for each of our halo samples, quoting subhalo masses as a fraction of the cluster virial mass. The flattening off and eventual decline of each distribution for decreasing subhalo masses is due to the minimum substructure mass in our simulation ( $7.62 \times 10^{11} h^{-1} M_\odot$ , or 30 particles). For subhalos with  $M_{sub} > 0.01 M_{vir}$  this effect appears not to be in evidence. Therefore, for subhalo masses greater than this, we fit a power-law –  $dN/d\log_{10}(M) = (M_{sub}/M_{vir})^\alpha$  – to the distributions, obtaining a slope of  $-0.79 \pm 0.04$  for the coherent sample (dashed lines) and  $-0.91 \pm 0.03$  for the standard halo sample (solid lines). Typically, most published studies have found that a power-law fit to the slope of the subhalo mass function results in values of  $\alpha$  between -0.7 and

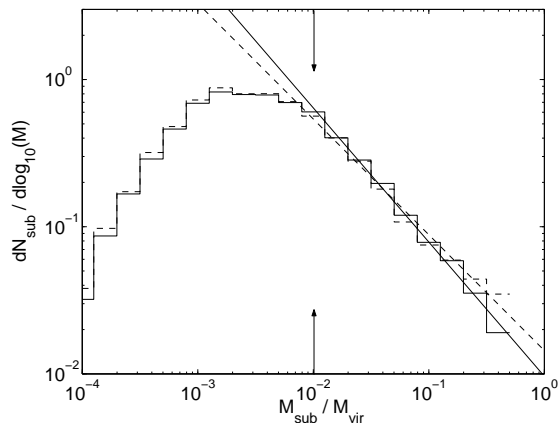


FIG. 10.— Mass distribution of all the subhalos in our coherent (dashed lines) and standard (solid) halo samples as a function of the ratio of subhalo to cluster halo mass. Straight lines are the power law fits to the slope outwards of the point indicated by the arrow, which is where we assume that the distribution is not affected by the minimum subhalo mass in our simulation (30 particles, or  $7.62 \times 10^{10} h^{-1} M_{\odot}$ ). Slopes of the fit are  $-0.79 \pm 0.04$  and  $-0.91 \pm 0.03$  for the coherent and standard distributions respectively.

-1.1 (Moore et al. 1999; Ghigna et al. 2000; Helmi et al. 2002; Gao et al. 2004; De Lucia et al. 2004; Shaw et al. 2006; van den Bosch et al. 2005). Our results are therefore well within the range measured by other authors.

In general, there is good agreement between the two halo samples, although there is a greater number of very high mass subhalos ( $M_{sub} > 0.2M_{vir}$ ) in the coherent sample, resulting in a shallower slope than measured for the standard sample. On average, these high mass subhalos tend to reside within slightly lower mass clusters ( $\langle M_{vir} \rangle \approx 1.5 \times 10^{14} M_{\odot}$ ) than for the entire sample ( $\langle M_{vir} \rangle \approx 3 \times 10^{14} M_{\odot}$ ). They are also typically located near to the cluster core, where the density of background particles – those bound only to the mother halo – is greater. In the coherent subhalo sample these halos will tend to be more massive than their counterparts in the standard sample, as we include the contribution of the background particles to the binding energy of a subhalo. Furthermore, they are not subjected to strong tidal forces from the halo core because they are located in lower mass halos.

Fig. 11 shows the circular velocity function (CVF) for subhalo maximum circular velocity as a fraction of halo maximum circular velocity,  $V_{smax}/V_{hmax}$ . The maximum circular velocity for both subhalos and halos was calculated using the 3 parameter fitting formula proposed by Stoehr (2006) (hereafter, STWS):

$$\log\left(\frac{V(x)}{V_{max}}\right) = -a[\log(x)]^2 \quad (11)$$

where  $x = r/r_{vmax}$  and  $V_{max}$ ,  $r_{vmax}$  and  $a$  are the maximum circular velocity, the radius at which this is located, and the width of the profile, respectively. We have adopted this profile because the flexibility provided by the additional free parameter compared to the NFW density profile (Navarro et al. 1996), results in a more accurate measure of the maximum circular velocity of a halo. We find that the STWS formula provides a good fit to the circular velocity profile of subhalos of at least 100 particles. Hence, in Fig. 11 we only use subhalos of at least this mass.

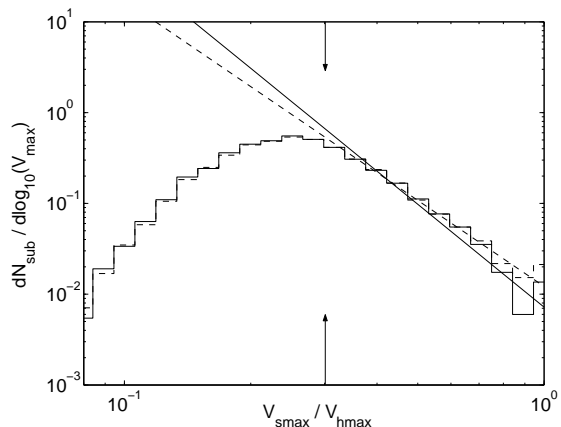


FIG. 11.— Maximum circular velocity distribution of all the subhalos in our coherent (dashed lines) and standard (solid) halo samples as a function of the ratio of subhalo to halo maximum circular velocity. Straight lines are the power law fits to the slope outwards of the point indicated by the arrow, which is where we assume that the distribution is not affected by the minimum subhalo mass to which we can reliably measure subhalo maximum circular velocity (100 particles, or  $2.54 \times 10^{11} M_{\odot}$ ). Slopes of the fit are  $-3.13 \pm 0.11$  and  $-3.66 \pm 0.30$  for the coherent and standard distributions respectively.

We fit a power-law to the distribution for  $V_{smax} > 0.3V_{hmax}$ , where it is less affected by the incompleteness effects of a minimum subhalo mass, obtaining a slope of  $-3.13 \pm 0.11$  for the coherent halo sample (dashed lines) and  $-3.66 \pm 0.30$  for the standard sample (solid lines). Reed et al. (2005) measure a slope of -4 for their sample of 16 high resolution subhalos, with significant scatter. The virial theorem gives the simple scaling relation,  $M \propto V_{max}^{\beta}$ , where  $\beta = 3$  for isolated halos. However, for subhalos having undergone mass loss, and because of a weak correlation between halo mass and concentration,  $\beta$  tends to vary between 3-4 (Avila-Reese et al. 1999; Bullock et al. 2001; Hayashi et al. 2003; Kravtsov et al. 2004b; Shaw et al. 2006). Hence, the relative values we obtain for the slopes of the SMF and CVF largely agree with what may be expected given the relationship between  $M_{vir}$  and  $V_{max}$ .

Overall, we again find a general good agreement between the two samples, with evidence of a slightly higher number of high  $V_{smax}$  subhalos in the coherent sample, resulting in the shallower slope. There is also a tiny fraction of subhalos with a greater maximum circular velocity than their host. These are very high mass subhalos –  $M_{sub} \approx 0.38M_{vir}$  – of almost equal mass to the mother halo itself. It is generally known that the maximum circular velocity is a quantity that is fairly robust to changes in subhalo mass due to dynamical friction and tidal stripping (e.g. Kravtsov et al. (2004b)). Hence, it is not necessarily surprising that we should find high mass subhalos with  $V_{smax}$  slightly greater than their hosts.

In Fig. 12 we compare the distributions of the total fraction of mass contained in substructure ( $f_s$ ) for both our halo samples. Aside from the slightly increased number of very high mass substructures (relative to their host halo mass) discussed earlier, there is a very good agreement between the two definitions of substructure. The mean value of  $f_s$  for the fully self-consistent definition of substructure halo sample is  $0.089 \pm 0.073$ , compared to  $0.082 \pm 0.066$  for the standard definition sample (errors

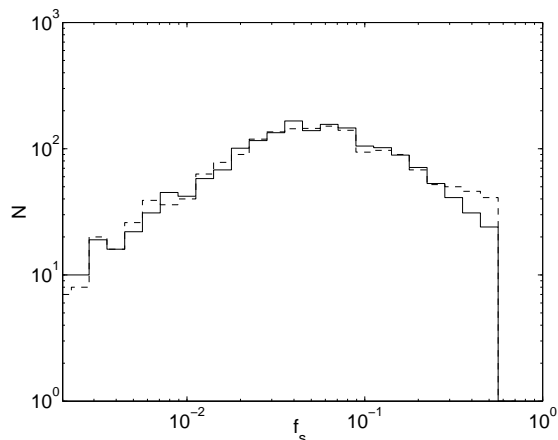


FIG. 12.— Distribution of the fraction of mass contained within substructure ( $f_s$ ) for all the halos in our coherent (dashed lines) and standard (solid) samples.

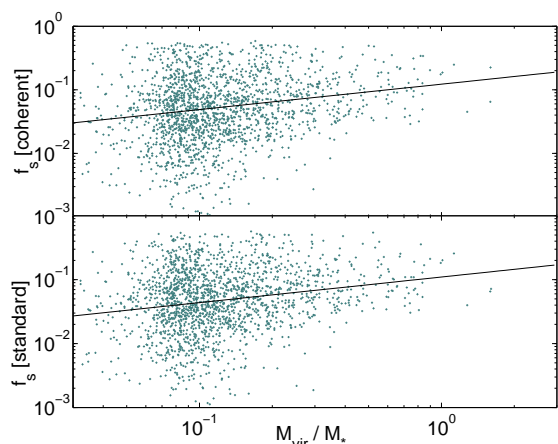


FIG. 13.— Fraction of mass contained within substructure as a function of halo mass, for our coherent halo sample (upper panel) and our standard halo sample (lower). Solid lines are the best fit power law to each distribution, where we obtain slopes of  $0.44 \pm 0.09$  and  $0.40 \pm 0.09$  for the coherent and standard samples respectively. We take  $M_*$  as  $8 \times 10^{14} M_\odot$ .

correspond to one standard deviation). These values also agree extremely well with those found in other studies (De Lucia et al. 2004; Gao et al. 2004; Gill et al. 2004b) who tend to find average values of  $f_s$  in the range 8-10%.

In Fig. 13 we plot  $f_s$  against halo mass for the coherent (top panel) and the standard (lower panel) halo samples. It is clear that for both samples that higher mass halos, on average, contain a higher fraction of their mass in substructure. To each distribution we fit a power law, obtaining similar slopes of  $0.44 \pm 0.09$  and  $0.40 \pm 0.09$  for the coherent and standard samples, respectively. This is an important result as it demonstrates that cluster-mass halos are not self-similar. Gao et al. (2004) found a similar result analyzing a reasonably large sample of halos over a wide mass range. van den Bosch et al. (2005) constructed a semi-analytical model to calculate the subhalo mass function, adjusting the free parameters to match the simulations of Gao et al. (2004), Tormen et al. (2004) and De Lucia et al. (2004); they found the slope and normalization of the mass function to be dependent on the ratio of halo mass to the characteristic non-

linear mass scale. In our previous paper (Shaw et al. 2006) we demonstrated that halos with a higher fraction of their mass contained in substructure typically also have a lower concentration, less spherical morphology and greater spin. We find the same results apply to the halos in our coherent sample.

Overall, we find that accounting for all the forces on a substructure, both internal (including the contribution of the ‘background’ particles to the binding energy) and external (incorporating the tidally disruptive effect of the cluster mass), does not produce a significantly different subhalo population from the definition of substructure used in previous studies. In the following section, we analyze and discuss the radial distributions of substructures in our halo samples.

### 3.2. Radial Distribution of Substructures

The simplest assumption one may make is that the radial distribution of satellite galaxies in a cluster follows the distribution of the dark matter. However, a number of recent studies investigating the radial distribution of subhalos in dissipationless simulations of cluster mass halos have found that this distribution is significantly less concentrated, and shallower in the inner regions, than that of the dark matter (Ghigna et al. 1998; Colín et al. 1999; Ghigna et al. 2000; Springel et al. 2001; De Lucia et al. 2004; Gao et al. 2004; Nagai & Kravtsov 2005; Reed et al. 2005; Faltenbacher & Diemand 2006). Diemand et al. (2004) performed convergence tests to show that the discrepancy between the dark matter density and subhalo radial distributions is likely not due to numerical resolution issues in the inner regions of halos; rather, it is that the destructive forces to which a subhalo is subjected (dynamical friction, tidal shocks, merging) proceed more rapidly in the inner regions than at the periphery of the system. Nagai & Kravtsov (2005) found in their simulations that whilst the radial distribution of subhalos was significantly less concentrated than that of the dark matter when selected using their present-day gravitationally bound mass, their radial distribution followed that of the dark matter much more closely when selected using their mass at the time of accretion. By performing simulations including gas dynamics, star formation and cooling, they also demonstrate that the radial distributions of subhalos selected by their stellar mass resulted in profiles similar in shape to that of the dark matter. As stars are located in the core of subhalos, and are therefore tightly bound, the stellar mass in a subhalo is a quantity that should not vary substantially over time.

In order to compare the radial distributions of substructure in each of our samples, in the upper panel of Fig. 14 we plot the spherically averaged fraction of mass in substructure within a given radius  $r$ ,  $f_s(< r/R_{vir})$ . This is calculated by dividing the mass in substructures by the total mass inside spheres of successively increasing fractions of the virial radius; we then take the mean value of all the halos in each sample at each radii. The circles/dashed line show the coherent halo sample, and the diamonds/solid line show the standard sample. For reference, we also plot the mean fraction of the total halo mass,  $M(< r/R_{vir})/M(R_{vir})$  within each radius (crosses/dotted line). In Fig. 15 we plot the *projected*

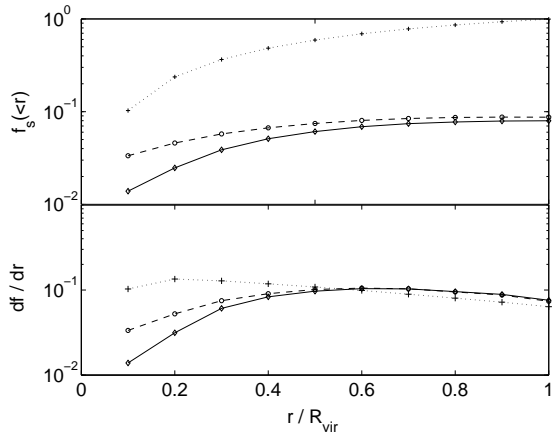


FIG. 14.— (*upper panel*) Cumulative fraction of mass in substructure within spheres of radius  $r/R_{vir}$ , for our coherent (dashed line) and standard (solid line) halo samples. Dotted line denotes the total mass contained with radius  $r$  as a fraction of the total halo mass at the virial radius. (*lower*) The fraction of mass in substructure in radial bins,  $df/dr = (M_{sub}(r+dr) - M_{sub}(r))/(M_{tot}(r+dr) - M_{tot}(r))$ , for both halo samples. For reference we also plot  $(M_{tot}(r+dr) - M_{tot}(r))/M_{vir}$  (dotted line).

radial distribution of the mass contained in substructure; this is calculated by taking the mean of three orthogonal projections of each halo. In the upper panel we plot the substructure mass within a projected fraction of the halo virial radius,  $R/R_{vir}$ , as a fraction of halo virial mass, or  $M_{sub}(<R)/M(R_{vir})$ , for the coherent (dashed line) and standard (solid) halo samples. For reference, we also plot the total halo mass within  $R/R_{vir}$  as a fraction of  $M_{vir}$  (dotted line). In the lower panel we plot the substructure mass within  $R/R_{vir}$  as a fraction of the total halo mass within  $R/R_{vir}$ , or  $M_{sub}(<R)/M_{DM}(<R)$ .

As found in previous studies, it is clear that the radial distribution of substructure does not follow that of the dark matter in the inner regions of a cluster. We re-emphasize that the minimum subhalo mass in each sample is 30 particles or  $7.62 \times 10^{10} h^{-1} M_{\odot}$  and the minimum cluster virial mass is 10,000 particles or  $2.54 \times 10^{13} h^{-1} M_{\odot}$ . Outward of  $0.6R_{vir}$ , the cumulative fraction of mass in substructure for both samples remains constant, indicating that in the outer regions the subhalos trace the overall dark matter distribution fairly well. Within this radius, the mass in subhalos relative to the dark matter decreases significantly. This is much more pronounced for the standard halo sample, which drops off much more steeply than the coherent sample. This is also shown in the lower panel of Fig. 14, where we plot the mean value of  $f_s$  for each sample in radial bins. This is calculated by dividing the mass in substructure between  $r$  and  $r+dr$  by the total halo mass within the same spherical annulus. For reference we also plot  $(M_{tot}(r+dr) - M_{tot}(r))/M_{vir}$  at each radii (dotted line). Outwards of  $0.5R_{vir}$  the results for each sample are very similar, but inside this radius there is significantly more substructure in the coherent halo sample. Thus in the inner regions of a halo, the binding effect of including the background (or unbound particles) located within a subhalo is on average slightly stronger than than the tidal forces from the cluster core and other surrounding substructures.

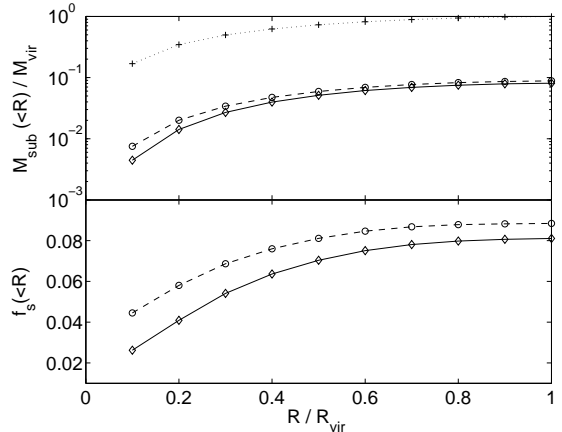


FIG. 15.— (*upper panel*) Cumulative projected subhalo mass for the coherent (dashed lines) and standard (solid lines) halo samples as a fraction of halo virial mass,  $M_{sub}(<R)/M(R_{vir})$ . Dotted line denotes the total halo mass contained within successively increasing fractions of the virial radius as a fraction of halo virial mass,  $M_{tot}(<R)/M(R_{vir})$ . (*lower panel*) Cumulative projected mass in substructure in circles of radius  $R/R_{vir}$  as a fraction of the total halo mass within the circular region,  $M_{sub}(<R)/M_{tot}(<R)$ .

### 3.3. Subhalos of subhalos

When a halo is accreted onto a more massive host, it may bring with it its own internal hierarchy of substructures. This is observed by Gill et al. (2004b), who follow the temporal evolution of satellites in their simulations as they are accreted by their host. Assuming this internal structure survives the initial impact of the disruptive environment within a cluster, we might expect that more massive halos will contain several generations of subhalos. Both Zentner et al. (2005) and Taylor & Babul (2004) try to account for subhalos-of-subhalos during their construction of semi-analytic models for the subhalo populations of dark matter halos.

We have performed a preliminary investigation of the amount of mass that is contained in subhalos that are not immediate daughters of the mother halo. Weller et al. (2005) describe in detail how the family-tree style hierarchy of substructures in each halo is calculated, depending on whether each subhalo is bound to the next most massive structure in the vicinity. Due to the resolution limits of our simulation, we are only able to resolve substructures down to a mass of approximately  $10^{-3} - 10^{-4}$  of the cluster halo virial mass. However, this is good enough to ensure that many of the cluster halos in each of our samples contain at least two generations of substructures. Indeed, several halos in our sample contain a small number of *third* generation subhalos.

We have previously defined  $f_s$  as the fraction of halo mass contained in substructure. We now also define  $f_{ss}$  as the fraction of mass in each subhalo contained in second generation subhalos. Of course, the minimum subhalo mass in our simulation,  $7.62 \times 10^{10} h^{-1} M_{\odot}$  or 30 particles, inhibits our ability to identify sub-subhalos in subhalos more than it does to identify subhalos in halos. Therefore we only include in our sample subhalos with masses of at least 1% that of their host halo, or  $M_{sub} \geq 0.01 M_{vir}$ , when calculating  $f_s$ , and second generation subhalos with  $M_{ss} \geq 0.01 M_{sub}$  when calculating  $f_{ss}$ . Additionally, we only analyze the sub-subhalo populations of subhalos that satisfy the first criterion, i.e.

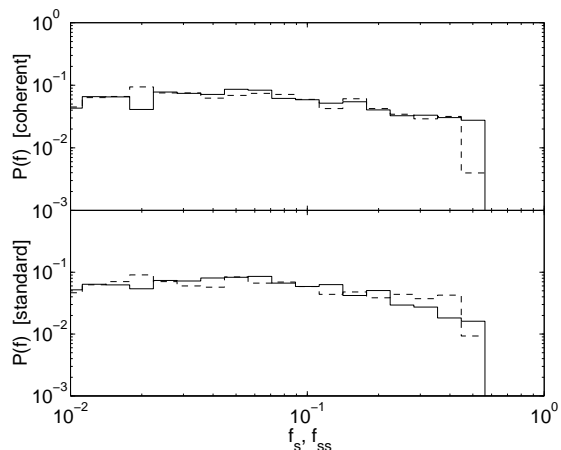


FIG. 16.— Distribution of the fraction of the halo mass contained within substructure,  $f_s$  (solid lines) and the fraction of subhalo mass contained within second generation subhalos,  $f_{ss}$  (dashed lines) for our coherent (*upper panel*) and standard (*lower panel*) halo samples. Distributions are normalized by the total number of halos for which  $f_s$  – and subhalos for which  $f_{ss}$  – is greater than zero.

$M_{sub} \geq 0.01 M_{vir}$ . All halos and subhalos that contain no subhalos or sub-subhalos, respectively, are discarded. We therefore now have a consistent means of comparing the populations of different generations of subhalos.

In the upper panel of Fig. 16 we compare the distribution of  $f_s$  for all the halos in our coherent sample (solid line) to the distribution of  $f_{ss}$  for all the *subhalos* in the entire sample (dashed line) in logarithmic bins. In the lower panel, we plot the equivalent distributions for the standard halo sample. We normalize each distribution so that it is expressed as a fraction of the total number of halos with  $f_s > 0$  for the former, and the number of halos with  $f_{ss} > 0$  for the latter. Hence, the distributions represent the probability of a halo containing  $f_s$  of its mass in substructure, and the probability of a subhalo containing  $f_{ss}$  of its mass in sub-substructure, assuming that both  $f_s$  and  $f_{ss}$  are greater than zero.

The similarity between the distributions of  $f_s$  and  $f_{ss}$  – especially for the coherent sample – is striking. It suggests a self-similarity within the hierarchical structures of cluster mass halos, with the 2nd generation of subhalos distributed in the 1st generation, as the latter is in the cluster as a whole. This result is both new and extremely interesting, especially considering that it has been demonstrated that halos are not self-similar – younger, higher mass halos tend to contain more substructure than their older, lower mass counterparts (Gao et al. 2004; Diemand et al. 2004; Shaw et al. 2006). However, it may not entirely be surprising. Just as recently formed halos contain a higher fraction of their mass in substructure, recently *accreted* subhalos might be expected to be the same – they have only recently become exposed to the disruptive environment within a halo, and so still retain a significant number of their own subhalos. Older halos have had more time to disrupt the substructures they host, so older subhalos will have lost a higher fraction of their own sub-subhalos due to the same processes. We hope to investigate this further with higher resolution simulations, enabling the identification of several generations of subhalos, in the near future.

#### 4. DISCUSSION AND CONCLUSION

In this paper we have presented a improved definition of subhalos in dissipationless dark matter N-body simulations, based on the coherent identification of their dynamically bound constituents. Whereas previous methods determine the energetically bound components of a subhalo while ignoring the contribution of particles in the halo that are not geometrically or dynamically associated with it, our method accounts for all the forces, both internal and external, exerted on a subhalo. This is realized in two stages: first, when calculating the energetically bound components of a subhalo, we include the contribution to the gravitational potential of those particles that were geometrically assigned to it, but that have been identified as unbound in previous iterations of the calculation. In previous studies, the contribution of unbound particles has been ignored. The effect of including their forces is to increase the binding energy, and therefore the mass of a subhalo. Second, we allow for the external forces exerted on each subhalo by the rest of the particles in the halo. This is achieved by approximating the tidal forces on each face of a cube surrounding each subhalo. We then calculate whether the tidal forces on each particle are sufficient to detach it from the subhalo within a characteristic time, discarding those for which this is the case. The effect of this stage therefore is to reduce the mass of subhalos – especially those near to the halo core or other dense conglomerates of particles.

To demonstrate that our new *coherent* method of identifying subhalos results in a more accurate measure of their bound mass than the standard procedure, we tracked two samples of approximately 50 subhalos over six consecutive timesteps (from  $z = 0.13$  to 0, or 1.17 Gyrs), identified using the coherent and standard methods respectively. By checking whether particles identified as bound to a subhalo (by either criterion) remained so, and whether nearby particles that were found not to be bound did indeed move away, we were able to assess how accurately each method identifies the bound mass of a subhalo. We demonstrated that the standard method is less successful at removing particles that are not bound to a subhalo. The average fraction of a subhalos mass that was identified as bound by the standard method but was found to have left the subhalo by the next timestep was, on average, a factor of 1.29 greater than that measured for the coherent method (9% compared to 7%). As expected, the accuracy of both methods decreases when we compare subhalos to their descendants several timesteps ahead; after 5 timesteps (1.17 Gyrs or  $\approx 14$  characteristic dynamical times) 28% and 25% of the particles identified as ‘bound’ by the standard and coherent methods respectively, were found to have left the subhalo.

We then applied both the standard method of identifying subhalos and our new coherent definition to a sample of 1838 virialized halos extracted from a high resolution cosmological simulation. We found the subhalo mass and maximum circular velocity distributions (relative to the mass and maximum circular velocity of their hosts) for each sample to be very similar. The slope of the high mass end of the subhalo mass distribution was  $-0.79 \pm 0.04$  and  $-0.91 \pm 0.03$  for the coherent and standard halo sample respectively. The slightly flatter slope

for the coherent sample was due to a small increase in the number of very high mass subhalos, relative to their host. We obtained equivalent slopes of  $-3.13 \pm 0.11$  and  $-3.66 \pm 0.30$  for the subhalo maximum circular velocity distributions. The mean fraction of mass contained in substructure,  $f_s$ , was  $0.089 \pm 0.074$  for the coherent halo sample and  $0.082 \pm 0.066$  for the standard sample. These results are all within the range of values found by previous authors.

In agreement with Gao et al. (2004), we find that  $f_s$  tends to increase with halo mass for both halo samples. High mass halos ( $M_{vir} > M_*$ ) have formed more recently and have therefore have had less time to disrupt the subhalos the halos they accreted. In our previous study (Shaw et al. 2006), we demonstrated that – for our *standard* halo sample – halos with a high  $f_s$  are typically also less spherical, have a lower concentration and a higher angular momentum than halos with a lower fraction of their mass in substructure. We have verified that the same is true for our coherent halo sample. These results break the assumption that is adopted in some semi-analytic models (e.g. Oguri & Lee 2004) that dark matter halos are self-similar, with galaxy mass halos resembling ‘miniature’ cluster mass halos. Recently, using a prescription for modelling the evolution of subhalos under the influence of dynamical fraction and tidal stripping, Zentner et al. (2005) and Taylor & Babul (2004) have developed semi-analytic models that correctly predict the deviations from a self-similar scaling of subhalo abundance with halo mass.

We then proceeded to investigate the radial distributions of substructure in each sample. We found that within 60% of the halo virial radius the distribution of subhalos is significantly less concentrated than that of the dark matter particles. However, this effect was less pronounced for subhalos in the coherent halo sample, indicating that in the central regions, the binding effect of including the ‘background particles’ in the potential calculation is slightly stronger than the disruptive effect of the tidal forces. This increases the mass of the subhalos in the inner regions of a halo relative to their counter-

parts in the standard halo sample.

Overall, however, we found that the inclusion of the contribution of ‘background’ particles to the binding energy of a subhalo was offset by the disruptive effect of the tidal forces from particles outside a subhalo. As these two effects, on average, tend to negate each other, we found that the subhalo populations were not substantially different to those found using the standard definition of substructure.

Finally, we performed a preliminary comparison of the subhalo population of halos to the second generation, or *sub-subhalo*, populations of subhalos. As part of our subhalo identification scheme, we construct for each halo a ‘family tree’ of substructure, checking to see whether smaller subhalos are bound to more massive subhalos. Our results indicate that the distribution of 2nd generation subhalos within their first generation hosts, mimics that of the distribution of subhalos in the overall halo. Hence, we find there to be a self-similar scaling between the populations of different generations of subhalos within halos. This is a new and interesting result, especially given the *lack* of self-similarity in the overall subhalo populations of host halos of different mass. We intend to investigate this further in the near future, with higher resolution simulations, and thus with halos containing multiple generations of subhalos.

## 5. ACKNOWLEDGMENTS

LDS acknowledges a PPARC student fellowship. This work was supported by a grant of supercomputing time (grant number MCA04N002P) from the National Center for Supercomputing Applications, and also used computational facilities supported by NSF grant AST-0216105. This work also made use of the COSMOS (SGI Altix 3700) supercomputer at DAMTP in Cambridge and on the Sun Sparc-based Throughput Engine at the Institute of Astronomy in Cambridge. Cosmos is a UK-CCC facility which is supported by HEFCE and PPARC. We thank Scott Tremaine for helpful discussions and the referee for many useful suggestions.

## REFERENCES

- Amara, A., Metcalf, R. B., Cox, T. J., & Ostriker, J. P. 2006, MNRAS, 367, 1367
- Avila-Reese, V., Firmani, C., Klypin, A., & Kravtsov, A. V. 1999, MNRAS, 310, 527
- Bertschinger, E. & Gelb, J. M. 1991, Computers in Physics, 5, 164
- Binney, J. & Tremaine, S. 1987, Galactic Dynamics (Princeton University Press, Princeton, NJ, USA)
- Bode, P., Ostriker, J., & Turok, N. 2001, ApJ, 556, 93
- Bode, P. & Ostriker, J. P. 2003, ApJS, 145, 1B
- Bullock, J. S., Kolatt, T. S., Sigad, Y., Somerville, R. S., Kravtsov, A. V., Klypin, A. A., Primack, J. R., & Dekel, A. 2001, MNRAS, 321, 559
- Colín, P., Klypin, A. A., Kravtsov, A. V., & Khokhlov, A. M. 1999, ApJ, 523, 32
- Das, S. & Ostriker, J. P. 2006, ApJ, 645, 1
- Davis, M., Efstathiou, G., Frenk, C. S., & White, S. D. M. 1985, ApJ, 292, 371
- De Lucia, G., Kauffmann, G., Springel, V., White, S. D. M., Lanzoni, B., Stoehr, F., Tormen, G., & Yoshida, N. 2004, MNRAS, 348, 333
- Diemand, J., Moore, B., & Stadel, J. 2004, MNRAS, 352, 535
- Eisenstein, D. J. & Hut, P. 1998, ApJ, 498, 137
- Faltenbacher, A. & Diemand, J. 2006, MNRAS, 369, 1698
- Gao, L., White, S. D. M., Jenkins, A., Stoehr, F., & Springel, V. 2004, MNRAS, 355, 819
- Gelb, J. M. & Bertschinger, E. 1994, ApJ, 436, 467
- Ghigna, S., Moore, B., Governato, F., Lake, G., Quinn, T., & Stadel, J. 1998, MNRAS, 300, 146
- . 2000, ApJ, 544, 616
- Gill, S. P. D., Knebe, A., & Gibson, B. K. 2004a, MNRAS, 351, 399
- Gill, S. P. D., Knebe, A., Gibson, B. K., & Dopita, M. A. 2004b, MNRAS, 351, 410
- Hagan, B., Ma, C.-P., & Kravtsov, A. V. 2005, ApJ, 633, 537
- Hayashi, E., Navarro, J. F., Taylor, J. E., Stadel, J., & Quinn, T. 2003, ApJ, 584, 541
- Helmi, A., White, S. D., & Springel, V. 2002, Phys. Rev. D, 66, 063502
- Hennawi, J. F., Dalal, N., Bode, P., & Ostriker, J. P. 2005, astro-ph/0506171
- Huchra, J. P. & Geller, M. J. 1982, ApJ, 257, 423
- Kang, X., Jing, Y. P., Mo, H. J., & Börner, G. 2005, ApJ, 631, 21
- Kazantzidis, S., Mayer, L., Mastropietro, C., Diemand, J., Stadel, J., & Moore, B. 2004, ApJ, 608, 663
- Kim, J. & Park, C. 2006, ApJ, 639, 600
- Klypin, A., Gottlöber, S., Kravtsov, A. V., & Khokhlov, A. M. 1999, ApJ, 516, 530

- Kravtsov, A. V., Berlind, A. A., Wechsler, R. H., Klypin, A. A., Gottlöber, S., Allgood, B., & Primack, J. R. 2004a, *ApJ*, 609, 35
- Kravtsov, A. V., Gnedin, O. Y., & Klypin, A. A. 2004b, *ApJ*, 609, 482
- Lacey, C. & Cole, S. 1994, *MNRAS*, 271, 676
- Lahav, O., Lilje, P. B., Primack, J. R., & Rees, M. J. 1991, *MNRAS*, 251, 128
- Mao, S., Jing, Y.-P., Ostriker, J. P., & Weller, J. 2004, *Astrophys. J.*, 604, L5
- Moore, B., Ghigna, S., Governato, F., Lake, G., Quinn, T., Stadel, J., & Tozzi, P. 1999, *ApJL*, 524, L19
- Moore, B., Katz, N., & Lake, G. 1996, *ApJ*, 457, 455
- Nagai, D. & Kravtsov, A. V. 2005, *ApJ*, 618, 557
- Navarro, J. F., Frenk, C. S., & White, S. D. M. 1996, *ApJ*, 462, 563
- Neyrinck, M. C., Gnedin, N. Y., & Hamilton, A. J. S. 2005, *MNRAS*, 356, 1222
- Oguri, M. & Lee, J. 2004, *MNRAS*, 355, 120
- Okamoto, T. & Habe, A. 1999, *ApJ*, 516, 591
- Reed, D., Governato, F., Quinn, T., Gardner, J., Stadel, J., & Lake, G. 2005, *MNRAS*, 359, 1537
- Shaw, L. D., Weller, J., Ostriker, J. P., & Bode, P. 2006, *ApJ*, 646, 815
- Springel, V., White, S. D. M., Tormen, G., & Kauffmann, G. 2001, *MNRAS*, 328, 726
- Stadel, J., Katz, N., Weinberg, D. H., & Hernquist, L. 1997, [www-hpcc.astro.washington.edu/tools/skid.html](http://www-hpcc.astro.washington.edu/tools/skid.html)
- Stadel, J. G. 2001, Ph.D. Thesis
- Stoehr, F. 2006, *MNRAS*, 365, 147
- Summers, F. J., Davis, M., & Evrard, A. E. 1995, *ApJ*, 454, 1
- Taffoni, G., Mayer, L., Colpi, M., & Governato, F. 2003, *MNRAS*, 341, 434
- Tasitsiomi, A., Kravtsov, A. V., Wechsler, R. H., & Primack, J. R. 2004, *ApJ*, 614, 533
- Taylor, J. E. & Babul, A. 2004, *MNRAS*, 348, 811
- Tormen, G., Moscardini, L., & Yoshida, N. 2004, *MNRAS*, 350, 1397
- Vale, A. & Ostriker, J. P. 2006, *MNRAS*, 371, 1173
- van den Bosch, F. C., Tormen, G., & Giocoli, C. 2005, *MNRAS*, 359, 1029
- van Kampen, E. 1995, *MNRAS*, 273, 295
- Wambsganss, J., Bode, P., & Ostriker, J. P. 2004, *Ap. J. Lett.*, 606, L93
- Weller, J., Ostriker, J. P., Bode, P., & Shaw, L. 2005, *MNRAS*, 364, 823
- White, S. D. M. 1976, *MNRAS*, 177, 717
- Zentner, A. R., Berlind, A. A., Bullock, J. S., Kravtsov, A. V., & Wechsler, R. H. 2005, *ApJ*, 624, 505